Sustainable Carbon Materials

https://doi.org/10.48130/scm-0025-0013

Original Research

Open Access

Machine learning analysis of oscillatory-turbulent heat transfer using carbon-based diamond nanofluids over MHD nonlinear wavy surfaces

Danial Habib[1], Caiyan Qin[1*], Yue Yang[1], Mingming Zhang[1] and Yuting Guo[2]

Received: 11 November 2025

Revised: 9 December 2025

Accepted: 18 December 2025

Published online: 29 January 2026

Abstract

This study presents a comprehensive numerical analysis of the oscillatory heat transfer and of turbulent-flow dynamics of carbon-based diamond-water nanofluids on a vertical nonlinear wavy surface under magnetohydrodynamic (MHD) effects. The work highlights the pivotal role of nanodiamonds, a class of carbon nanomaterial characterized by ultra-high thermal conductivity (1,000 W/m·K) and exceptional stability, in enhancing thermal performance. The resulting governing flow model, derived using similarity transformations, is solved by the Keller-box method (KBM) and validated with exceptional accuracy (MSE $\approx 10^{-7}$) using an artificial neural network (ANN) for machine learning (ML). Aggregated (ANP) and non-aggregated nanoparticle (NANP) configurations are systematically studied under the rising magnetic field strengths (M = 1.0–5.0) and sinusoidal conditions (ε_T = 0.1–0.3). The results show that the formation of ANPs leads to a substantial increase in thermal conductivity due to the formation of conductive clusters, which increase the Nusselt number Nu by 30%, albeit at the considerable cost of a 25% increase in viscous dissipation and skin friction C_f. Conversely, non-aggregated nano-diamonds promote smooth velocity profiles that yield moderate enhancement in *Nu* (up to 22%) and high hydrodynamic functionality. Surface undulations generate oscillatory thermal dynamics and turbulent mixing structures, resulting in a 15%–20% reduction in the overall Nu due to boundary layer discontinuity. However, this negates the reduction resulting from the increase in overall thermal bridging. An optimal nanoparticle volume fraction C_f of 2%–3% is identified, balancing the thermal enhancement against the pumping power requirements. These results provide important design insights for advanced thermal management systems, especially in the cooling of electronics and high-performance heat exchangers, where magnetic field control and surface geometry optimization are critical for operational efficiency.

Keywords: Oscillatory heat transfer, Non-linear wavy surface, Nanoparticle clustering (NC), Diamond-water nanofluid, Artificial neural networks, Sinusoidal boundary conditions.

Highlights

- Nonlinear wavy surfaces induce oscillatory heat transfer and turbulent-like dynamics in MHD carbon-based nanofluids.
- Carbon-based diamond aggregated nanofluids enhance thermal conductivity, boosting the Nusselt number by 30% despite 25% higher viscous dissipation.
- A machine learning analysis hybrid Keller-Box framework achieves exceptional accuracy (MSE $\approx 10^{-7}$).
- Surface undulations reduce heat transfer by 15%–20%, but aggregation mitigates this through conductive networks.
- Optimal performance occurs at 2%–3% nanoparticle volume fraction and moderate magnetic fields (M = 2.3–3.4).
- Non-aggregated nanoparticles provide better hydrodynamic performance for flow-sensitive applications.

* Correspondence: Caiyan Qin (qincaiyan@hit.edu.cn)

Full list of author information is available at the end of the article.

https://doi.org/10.48130/scm-0025-0013

Graphical abstract

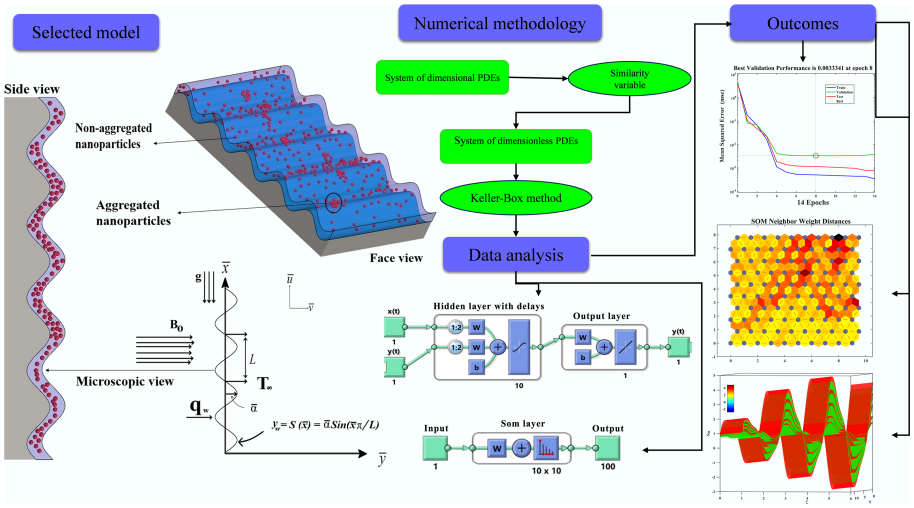

Introduction

In thermal engineering, fluids serve as the principal medium for energy transport, spanning applications from planetary climate systems to microscale cooling in electronic devices. The efficient design of radiators, heat exchangers, and microscale thermal management systems depends on the capacity of the fluid to store, transfer, and dissipate thermal energy. Advances in computational fluid dynamics have enabled modelling of flow dynamics and temperature fields, and heat transfer efficiency, thus reducing reliance on expensive and time-consuming experimental systems. The development of nanofluids, colloidal suspensions of nanoparticles in base fluids, has provided a new category of high-performance heat transfer media characterized by high thermal conductivity and low energy consumption by Zhang et al. and Doost et al.[1,2]. The evolution of nanofluids represents a remarkable leap in thermal engineering capabilities. Shah et al.[3] show their efforts in solar thermal engineering systems, utilizing the thermophysical properties of nanoparticles, and Timofeeva et al.[4] present a comprehensive description of the engineering approach to advanced heat transfer. Recent work highlights the potential for transformation in renewable energy sectors, extending to electronics cooling with nanofluids offered by Sohel et al. and Santhosh et al.[5,6].

Nanofluids are an important technological advancement in thermal engineering, engineered colloidal suspensions developed by dispersing nanoparticles in the traditional base fluids, like water, ethylene glycol, or oil. This idea, initially proposed by Choi[7], proved that the nanoscale additives could significantly improve the physical characteristics and heat conduction of the fluids regarding their thermophysical properties. The effectiveness of nanofluids depends on nanoparticle attributes, such as material type, morphology, size, and concentration, which collectively influence density, viscosity, specific heat, and thermal conductivity. The synergy of nanoparticles with the underlying fluid has led to the development of hybrid nanofluids, in which two or more species of nanoparticles are combined to enhance thermal functioning in an even larger way. These novel fluids are characterized by better energy carrier properties and have been used in a variety of applications, such as automotive cooling, petroleum processing, thermal management of electronic equipment, and renewable energy systems, particularly in the development of efficient thermoelectric performance of direct absorption solar collectors. Yasmin et al.[8] experimentally verified the use of hybrid nanofluids in thermal and solar energy storage, and Heidarshenas et al.[9] studied the stability and thermophysical behavior of two-dimensional nanomaterials. Thus, understanding and controlling aggregation is crucial in applications like cooling, biomedical systems, and heat exchangers. Subsequent research has compared aggregated and non-aggregated nanoparticles at elevated temperatures in cylindrical geometries by Ramzan et al.[10] and developed models to assess anisotropic conductivity effects by Wu et al.[11]. Mudhukesh et al.[12] studied radiation effects on magnetically aggregated nanoparticles and applied multiscale MD-LBM methods to analyze molten salt nanofluids with aggregated particles by Yang et al.[13].

Convective heat transfer on sinusoidal surfaces is well known to promote convection heat transfer by discontinuously disrupting the thermal boundary layer, which facilitates fluid mixing as well as increasing the thermal efficiency in each direction. It is widely recognized that wave or non-uniform surfaces may greatly enhance heat transfer, as they disrupt the thermal boundary layer and cause fluid mixing. This principle is the foundation of superior cooling techniques in electronics, biomedical devices, and miniature energy equipment. Recent interest has focused on the thermomagnetic effects of such geometries, which has attracted the attention of researchers[14–16] who discovered different wave structures and convection patterns. For example, Iqbal et al.[17,18] investigated the interaction of magnetic and thermal fields, and Akter et al. and Munir et al.[19,20] considered how the inclusion of a magnetic field can influence thermal performance. Practically speaking, the wavy heat exchangers have been particularly useful in augmenting circulation and heat distribution in fluids, thus decreasing thermal stresses and enhancing the overall efficiency of energy use[21–23].

The physical configuration of the wavy-surfaced porous medium solar collector and computational mesh, and boundary conditions are depicted in Fig. 1[24–28]. In the physical model illustrated in Fig. 1a, the saturation of a wavy absorber surface with nanofluid is represented, and heat transfer is achieved by absorbing solar energy at the top and surface of the heated material, radiative cooling, and convectional exchange with the surrounding air. Figure 1b presents

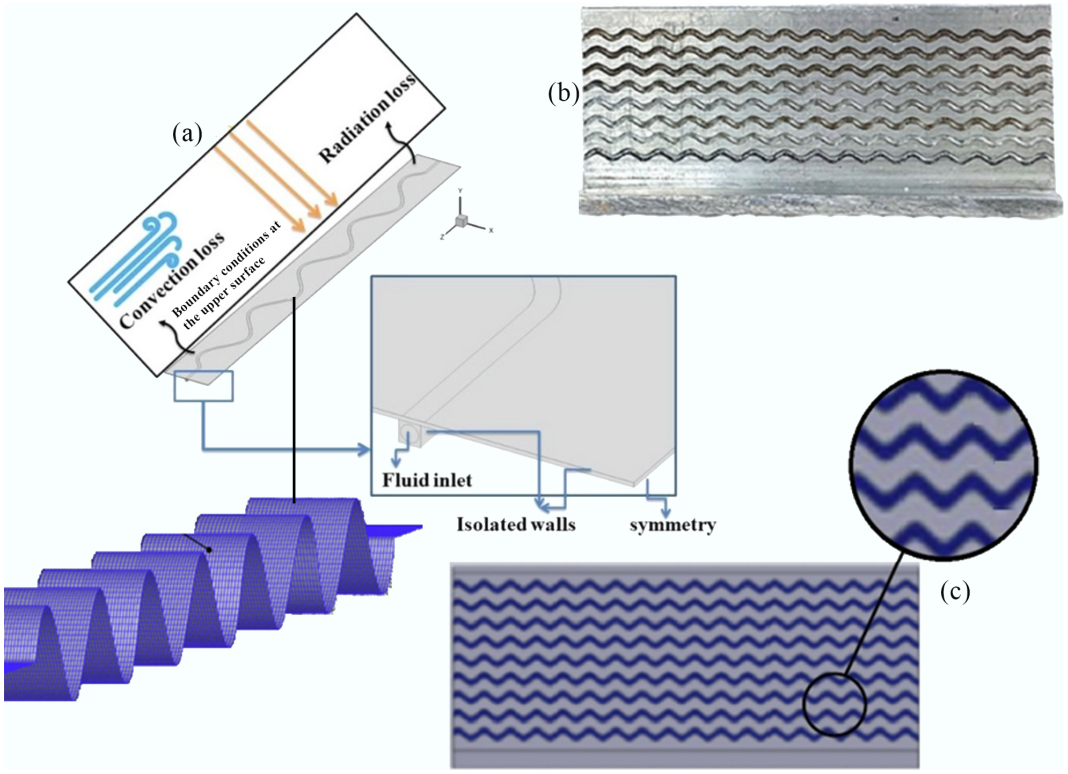

Fig. 1 Schematic representation of the physical model and computational domain with a sinusoidal surface. (**a**) Heat transfer mechanisms and loss components. (**b**) Boundary conditions and symmetry setup. (**c**) Overall system configuration.

the wavy absorber plate used in the experimental or modeled setup, highlighting the structured surface geometry that enhances heat transfer performance. Figure 1c demonstrates the computational mesh and boundary conditions, such as an adiabatic bottom wall, symmetrical side lateral walls, a nanofluid inlet with specified velocity and temperature, and an upper surface that has convective and radiative heat losses. These sub-figures define the problem domain, mesh strategy, and thermal boundary constraints employed in the numerical analysis.

Growing global energy demands have made the optimization of heat exchangers a critical priority in thermal system design. ANNs have become potent predictors of the behavior of heat transfer and system optimization to reduce system efficiency, providing high accuracy with minimal computational cost through their ability to learn from complex input data sets. The trend is shown by their recent research, where ANN modeling was used for hybrid nanofluids and for the optimization of polymer microchannels by Ain et al.[29] and Kamsuwan et al.[30], respectively. Other studies have analyzed radiative Jeffrey nanofluid flow by Zeeshan et al.[31], and Islam et al.[32] applied ANN to the response surface methodology. Subsequent works include those by Bilal et al.[33], which provided numerical and experimental confirmation of ANN-based models, and Ali et al.[34], which provided subsequent confirmation through numerical and experimental validation. Additional advancements highlight the versatility of machine learning in thermal systems. A study on material selection and optimization of hybrid solar-thermal plume systems to enhance passive cooling and energy efficiency was presented for materials in 2025 by Yahya et al.[35]. A methodology for the radiative heat transport of nanofluids over a vertical cylinder is presented by Mahanthesh & Thriveni[36]. The simulation-driven optimization of direct solar dryers using a combined CFD and ANN-GA approach was demonstrated by Loksupapaiboon et al.[37].

Although significant progress has been made in understanding nanofluid heat transfer phenomena, the influence of nanoparticle properties, especially Lorentz forces and clustering performance under complex wavy surfaces, has received limited attention, as most investigations examine these factors individually. To fill this gap, the current study develops a robust Keller-box numerical framework to analyze MHD flow and oscillatory heat transfer of a carbon nanofluid over a wavy surface. By systematically evaluating both aggregated and non-aggregated nanoparticles under flexible magnetic fields and sinusoidal boundary conditions, this effort delivers practical insights relevant to industrial thermal management. Motivated by the need to augment thermal performance in geometrically complex, magnetically assisted cooling classifications, the current work has direct significance for high-flux cooling of compact heat exchangers in aerospace thermal management, power electronics (e.g., CPUs, IGBTs), and advanced solar collectors. The prime objectives are: (1) to assess the coupled effects of surface waves on nanoparticle aggregation, MHD forces, and oscillatory heat transfer; (2) to analyze the trade-off between hydrodynamic penalty and thermal enhancement; and (3) to develop a fast, accurate machine learning model for predictive analysis. This work fills the existing gap by:

- Developing a viscosity model that incorporates a modified thermal conductivity model for magnetic fields and sinusoidal surface parameters;
- Leveraging the high-fidelity KBM data to train an accurate ANN surrogate model for fast performance prediction and optimization with an MSE of ~10^{-7}).

https://doi.org/10.48130/scm-0025-0013

Mathematical modeling of the problem

This study investigates steady, laminar free convection of an incompressible nanofluid along a vertically oriented wavy surface with constant heat flux, under the influence of a transverse magnetic field. Assuming a low Reynolds number, the induced magnetic field is negligible. The formulation incorporates Lorentz forces and sinusoidal boundary conditions to represent natural convection influenced by magnetohydrodynamic (MHD) effects and surface undulations. The wavy surface is defined by $Y_w = \overline{\alpha}\sin(\pi\overline{x}/L)$, where $\overline{\alpha}$ and L are the amplitude and wavelength, respectively, as shown in Fig. 2. The governing equations for continuity, momentum, and energy are given as[17,38]:

$$\nabla.V = 0, \tag{1}$$

$$(V.\nabla)V = -\frac{1}{\rho_{nf}}\nabla p + \nabla^2 V + \frac{(\rho\beta)_{nf}}{\rho_{nf}}g(T-T_\infty) - \frac{\sigma_{nf}B_0}{\rho_{nf}}V, \tag{2}$$

$$V.\nabla T = \alpha_{nf}\nabla^2 T, \tag{3}$$

$$\left.\begin{aligned} &y = S(\overline{x}):\ \overline{u} = \overline{v} = 0,\ T = T_\infty + (T_w - T_\infty)\left[1 + \varepsilon_T \sin\left(\frac{\pi\overline{x}}{L}\right)\right], \\ &y \to \infty:\ \overline{u} = 0,\ p = p_\infty,\ T = T_\infty \end{aligned}\right\} \tag{4}$$

where, p denotes the fluid pressure, with p_∞ representing the ambient pressure and T indicating the temperature field. The nanofluid properties, including electrical conductivity and density, are represented by σ and ρ, respectively. A uniform magnetic field of strength B_0 is applied perpendicular to the wavy surface, assuming a sufficiently small magnetic Reynolds number to neglect the induced magnetic field.

$$\begin{aligned} &\psi(\xi,\eta) = \xi^{3/4} f(\xi,\eta), \quad \xi = \frac{x}{l}, \quad \eta = \xi^{-1/4} y, \\ &v = \frac{\rho_{nf}}{\mu_f} Gr^{-1/4}\left(\overline{v} - S_\xi \overline{u}\right), \quad S = \frac{S(\overline{x})}{l} = \overline{\alpha}\sin(\pi\xi), \\ &\Omega = \sqrt{1 + S_\xi^2}, \quad \theta(\xi,\eta) = \frac{T - T_\infty}{T_w - T_\infty}, \quad u = \frac{\rho_{nf}}{\mu_f} Gr^{-1/2}\overline{u}, \\ &\overline{v} = -\frac{\partial\psi}{\partial\overline{x}}, \quad y = \frac{y - S(\overline{x})}{l} Gr^{1/4}, \quad M = \frac{Ql^2}{\mu_f Gr^{1/2}\left(\rho c_p\right)_f}, \\ &\overline{u} = -\frac{\partial\psi}{\partial\overline{y}}, \quad P = \frac{l^2}{\nu^2\rho_f} Gr^{-1/4} p, \quad Gr = \frac{g\beta_f (T_w - T_\infty) l^3}{\nu_f^2}, \end{aligned} \tag{5}$$

The wall temperature is prescribed as $T_w(x)$, where T_w is the mean wall temperature, and T_∞ is the ambient fluid temperature, satisfying $T_w > T_\infty$ and modulated by the sinusoidal parameter ε_T. Here, $\alpha = \overline{\alpha}/L$ define the dimensionless surface amplitude of temperature oscillation, and L corresponds to the chrematistic wavelength, while ∇^2 represents the Laplacian operator. A set of appropriate dimensionless variables is introduced to facilitate the analysis. The velocity components along the (x, y) direction is $V = (\overline{u}, \overline{v})$. Using the above set of transformations, Eq. (5), leads to a dimensionless system of Eqs (6) and (7), and based on the boundary layer assumptions, Eq. (8), which can be written as:

$$\frac{\Omega^2}{D_1} f''' + \frac{3}{4} f f'' - \xi\left(\frac{1}{2} + \frac{\Omega_\xi}{\Omega}\xi\right)(f')^2 - \xi^{1/2}\left(\frac{MD_4}{D_2\Omega^2}\right) f' - \frac{D_4}{D_2\Omega^2}\theta = \xi\left[f'\frac{\partial f'}{\partial\xi} - f''\frac{\partial f}{\partial\xi}\right], \tag{6}$$

$$\frac{\Omega^2}{D_3\,\mathrm{Pr}}\theta'' + \frac{3}{4} f\theta = \xi\left[f'\frac{\partial\theta}{\partial\xi} - \theta'\frac{\partial f}{\partial\xi}\right], \tag{7}$$

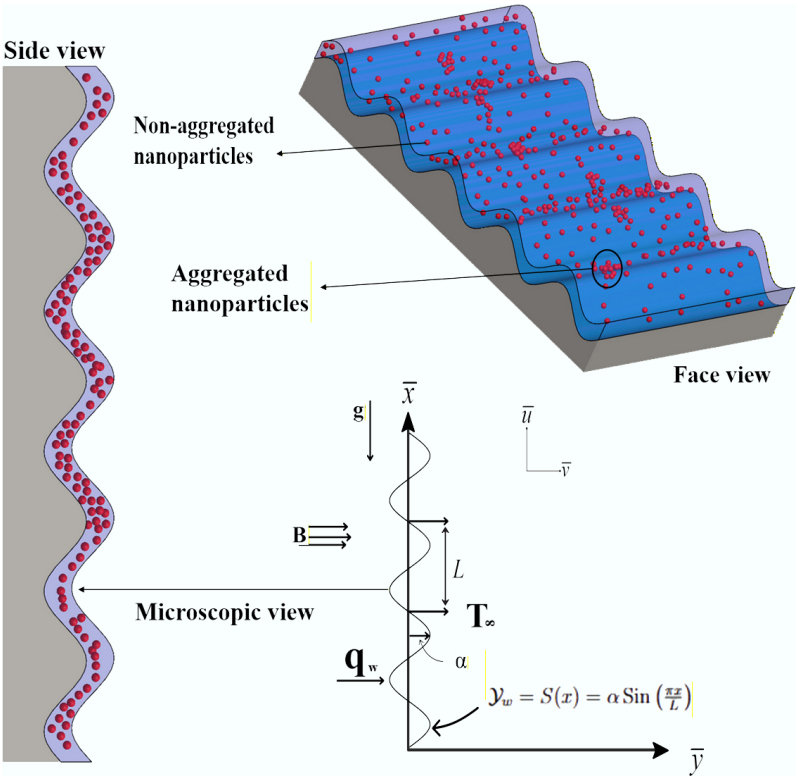

Fig. 2 Geometrical configuration of nanoparticle clustering near a sinusoidal surface.

$$\left.\begin{array}{l}\eta \to 0: \quad f(\xi,\eta)=0,\ \ f'(\xi,\eta)=0,\ \ \theta(\xi)=\left[1+\varepsilon_T \sin(\pi\xi)\right],\\ \eta \to \infty: \quad f'(\xi,\eta)=0,\ \ \theta(\xi,\eta)=0\end{array}\right\} \tag{8}$$

where, the Prandtl and magnetic numbers are denoted by *Pr* and *M*, respectively. The subscript ξ indicates differentiation concerning ξ, while the prime symbol (′) denotes differentiation for η. The parameter Ω represents the wavy surface effect in the governing equations.

The constants D_1, D_2, D_3, D_4, and D are nanofluid-specific parameters listed in Table 1. By employing Eq. (5), the local skin friction coefficient (C_f) and the local Nusselt number (Nu) in nondimensional form are expressed as follows. Table 2 Assumed values of physical quantities for scenario construction[37].

$$C_f = C_{f\bar{x}}(Gr/\bar{x})^{1/4} = \frac{\Omega}{(1-\phi)^{2.5}} f''(\xi,0), \tag{9}$$

$$Nu = Nu_{\bar{x}}\left(Gr\bar{x}^3\right)^{-1/4} = \Omega\frac{k_{nf}}{k_f}\theta'(\xi,0), \tag{10}$$

The current study uses a model of an artificial neural network (ANN) to estimate velocity and temperature distributions in different surface profiles with changing magnetic field strength, which is explained in Table 2 inspired by Kamsuwan et al.[30]. Two configurations are analyzed:

• Configuration A: Non-aggregated nanoparticles with variations in magnetic and sinusoidal parameters.

• Configuration B: Aggregated nanoparticles considering the combined influence of magnetic and sinusoidal parameters.

The study further explores two comparative scenarios:

• Scenario (I) (A, B): Cases 1–3 investigate the influence of magnetic field intensity.

• Scenario (II) (A, B): Cases 1–3 analyze the effects of sinusoidal surface parameters.

The dispersions of monodisperse diamond nanoparticles (20–50 nm) in water are due to their high thermal conductivity (1,000 W/m·K), chemical stability, and low aggregation propensity under (MHD) conditions. Diamond is also ideal because it has better heat transfer properties than metallic nanoparticles and is thus suited to high-precision uses, including aerospace cooling and power electronics.

The classical Maxwell and Brinkman models are used to compute the effective thermophysical properties, such as thermal conductivity and viscosity, with simplified results summarized in Tables 1 and 3 presents the effective thermophysical models for aggregated and non-aggregated nanoparticles by Mahanthesh et al.[36,40]. Aggregation impacts key properties such as viscosity, density, and thermal conductivity. Fractal-based models account for nanoparticle clustering, capturing irregular geometries and nanolayer effects that enhance heat transfer. Other factors like nanolayer thickness, cluster diameter, and interfacial resistance influence the overall conductivity, especially under nanoscale confinement by Prasher et al. and Evans et al.[41,42]. Additionally, viscosity decreases with rising temperature, as reported by Salahuddin et al.[43].

Numerical methodology

An implicit finite difference scheme based on the KBM by Keller and Cebeci & Bradshaw[44,45] is used to solve the governing partial differential Eqs (6) and (7) with boundary conditions Eq. (8). It provides second-order accuracy and numerical stability in highly nonlinear

Table 1 Thermophysical properties of aggregated and non-aggregated nanoparticles by Mahanthesh et al.[36]

Property	Constant	Non-aggregation	Aggregated
Viscosity μ	D_1	$\mu_{nf} = \mu_f(1-\varphi)^{-2.5}$	$\mu_{nf} = \mu_f\left(\frac{\phi_m-\phi_a}{\phi_m}\right)^{\phi_m}$
Density ρ	D_2	$\rho_{nf} = \rho_f\left[(1-\phi)+\phi\left(\frac{\rho_s}{\rho_f}\right)\right]$	$\rho_{nf} = \rho_f\left[(1-\phi_a)+\phi_a\left(\frac{\rho_s}{\rho_f}\right)\right]$
Specific heat capacity C_p	D_3	$(\rho C_P)_{nf} = (\rho C_P)_f\left[(1-\phi)+\frac{(\rho C_P)_s}{(\rho C_P)_f}\phi\right]$	$(\rho C_P)_{nf} = (\rho C_P)_f\left[(1-\phi_a)+\frac{(\rho C_P)_s}{(\rho C_P)_f}\phi_a\right]$
Thermal conductivity k	D_4	$k_{nf} = \left[\frac{\left(k_s+2k_f\right)-2\phi\left(k_f-k_s\right)}{\left(k_s+2k_f\right)+\phi\left(k_f-k_s\right)}\right]k_f$	$k_{nf} = \left[\frac{\left(k_s+2k_f\right)-2\phi_a\left(k_f-k_s\right)}{\left(k_s+2k_f\right)+\phi_a\left(k_f-k_s\right)}\right]k_f$
Electrical conductivity σ	D_5	$\sigma_{nf} = \sigma_f+\sigma_f\left[\frac{3\left(\frac{\sigma_s}{\sigma_f}-1\right)\phi}{\left(\frac{\sigma_s}{\sigma_f}+2\right)-\left(\frac{\sigma_s}{\sigma_f}-1\right)\phi}\right]$	$\sigma_{nf} = \sigma_f+\sigma_f\left[\frac{3\left(\frac{\sigma_s}{\sigma_f}-1\right)\phi_a}{\left(\frac{\sigma_s}{\sigma_f}+2\right)-\left(\frac{\sigma_s}{\sigma_f}-1\right)\phi_a}\right]$

Table 2 Parameter sets for scenario construction

A. Non-aggregated		B. Aggregated		
Scenario	Case	Selected parameters		
		M	ε_T	Description
I (A, B)	1	1	0.5	Weak magnetism over a wavy boundary
	2	2	0.5	Moderate field, typical in electronics cooling
	3	3	0.5	High-intensity field (advanced heat exchangers)
II (A, B)	1	4	1	Flat surface (baseline waviness)
	2	4	2	Moderate waviness boosts fluid mixing
	3	4	3	High undulation resembling turbulence

Table 3 Thermophysical properties of the considered nanoparticles by Sundar et al.[39]

Property	Base fluid	Nanoparticle
	Pure water	Diamond
μ (Pas)	0.000803	–
Density ρ (kg/m^3)	997.1	3,510
Specific heat capacity C_p (J/kg·K)	6.13×10^{-1}	497.26
Thermal conductivity k (W/m·K)	4,179	1,000
Average size	–	30 nm
Range	–	20–50 nm
Purity	–	> 95%

https://doi.org/10.48130/scm-0025-0013

systems. The computational domain is discretized via uniform steps in both the η and ξ directions based on a sound grid independence study. The solution procedure involves the following.

• Transformation of higher-order PDEs to first-order systems through variable substitution:

• Discretization using central differences with step sizes $\Delta\eta = \Delta\xi = 0.005$

• Linearization of resulting algebraic equations via Newton's method

• Solution of the linear system through block tri-diagonal elimination

$$f' = r,\ \ q = f'',\ \ t = \theta', \tag{11}$$

By applying Eq. (11), the transformed forms of the governing Eqs (6) and (7) are derived as follows:

$$\frac{\Omega^2}{D_1}q' + \frac{3}{4}fq - \xi\left(\frac{1}{2} + \frac{\Omega_\xi}{\Omega}\xi\right)(r)^2 - \xi^{1/2}\left(\frac{MD_4}{D_2\Omega^2}\right)r - \frac{D_4}{D_2\Omega^2}\theta = \xi\left[r\frac{\partial f'}{\partial \xi} - q\frac{\partial f}{\partial \xi}\right], \tag{12}$$

$$\frac{\Omega^2}{D_3\,\mathrm{Pr}}t' + \frac{3}{4}f\theta = \xi\left[r\frac{\partial \theta}{\partial \xi} - t\frac{\partial f}{\partial \xi}\right], \tag{13}$$

Boundary conditions and grid discretization

By applying Eq. (11), the transformed boundary conditions corresponding to Eq. (8) are obtained as follows.

$$\left.\begin{array}{l} f(\xi,0) = 0,\ \ r(\xi,0) = 0,\ \ \theta(\xi,0) = [1 + \varepsilon_T \sin(\pi\xi)], \\ f'(\xi,\infty) = 0,\ \ \theta(\xi,\infty) = 0 \end{array}\right\} \tag{14}$$

The computational grid is constructed with

$$\left.\begin{array}{ll} \xi^0 = 0, & \xi^n = \xi^{n-1} + k_n \\ \eta_0 = 0, & \eta_j = \eta_{j-1} + h_j \end{array}\right\} \tag{15}$$

for η, j = 1, 2, 3,…, N, where N_η = 3,000, and N_ξ = 400 grid points are used in the respective directions. Finite-difference approximations and Newton linearization are applied to the nonlinear system employed as follows:

$$\begin{aligned} ()_j^{n-0.5} &= 0.5\left[()_j^n + ()_j^{n-1}\right] \\ ()_{j-0.5}^{n} &= 0.5\left[()_j^n + ()_{j-1}^{n}\right] \end{aligned} \tag{16}$$

$$\begin{aligned} f_j^{i+1} &= f_j^i + \delta f_j^i \\ r_j^{i+1} &= r_j^i + \delta r_j^i \\ \theta_j^{i+1} &= \theta_j^i + \delta\theta_j^i \end{aligned} \tag{17}$$

The linearized system is solved using a block tri-diagonal algorithm with a convergence criterionof $\|\delta\|_\infty < 10^{-6}$.

Validation and verification

Numerical accuracy is ensured through

• Conservation checks for mass, momentum, and energy

• A grid independence study, as detailed in Table 4.

To guarantee that the numerical predictions are independent of spatial resolution, a grid convergence study was performed as Iqbal et al.[17]. The computational domain was discretized using progressively refined meshes ranging from 100 × 10 to 1,600 × 200 elements. Special mesh refinement was applied near the wavy wall (η = 20) and (ξ = 1.0) to resolve steep velocity and temperature gradients.

The grid sensitivity was assessed through the skin friction coefficient C_f and local Nusselt number (Nu). Results obtained using an 800 × 100 to 1,600 × 200 mesh differed by less than 0.0001% from those computed with a 1,600 × 200 mesh, confirming grid independence. Hence, all subsequent simulations were conducted on the 1,600 × 200 grid. Table 4 presents the normalized C_f and Nu distributions for various mesh densities, reaffirming the adequacy of the selected grid resolution.

Table 4 Grid independence test for $\phi = 0.0$, $Pr = 0.62$, $\alpha = 0.1$, and $M = 0.2$

Number of grid points		Output	
η- direction (With fixed η = 20)	**ξ- direction (With fixed ξ = 1)**	**C_f**	**Nu**
100	10	−0.85351	0.31688
200	20	−0.85381	0.31699
400	50	−0.85392	0.31680
800	100	−0.85392	0.31680
1,600	200	−0.85382	0.31680

Machine learning (ANN) methodology

Artificial neural networks are feedforward networks trained with the Levenberg-Marquardt backpropagation algorithm. This study consisted of an input layer (configuration M, ε_T), one hidden layer with ten neurons (tanh activation), and an output layer (Nu, C_f). The dataset from the KBM simulation is split into 70%–15%–15% for training, validation, and testing, respectively. Premature stopping based on validation error is used to prevent overfitting. Detailed performance metrics (MSE, epochs) for all scenarios are provided in Table 5.

Table 5 Outcomes of all scenarios with ANNs and LMT

Scenario		Case	MSE data			Performance	Gradient	Mu	Final epoch	Time (s)
			Training	Validation	Testing					
Non-aggregated	I A	1	$1.48882e^{-5}$	$3.23527e^{-5}$	$1.38677e^{-5}$	$1.21e^{-5}$	$1.00e^{-7}$	$1e^{10}$	25	< 1
		2	$1.48550e^{-5}$	$3.32879e^{-5}$	$1.47673e^{-5}$	$1.20e^{-5}$	$1.92e^{-8}$	$1e^{10}$	67	< 2
		3	$1.72843e^{-5}$	$3.13655e^{-5}$	$1.32171e^{-5}$	$1.03e^{-5}$	$1.98e^{-7}$	$1e^{10}$	99	< 3
	II A	1	$4.35370e^{-6}$	$4.65936e^{-5}$	$4.34532e^{-5}$	$4.09e^{-6}$	$9.99e^{-08}$	$1e^{-6}$	93	6
		2	$4.89685e^{-6}$	$4.54796e^{-5}$	$4.58981e^{-5}$	$3.89e^{-6}$	$9.92e^{-08}$	$1e^{-6}$	104	4
		3	$4.52364e^{-6}$	$4.85467e^{-5}$	$5.41256e^{-5}$	$4.89e^{-6}$	$9.98e^{-08}$	$1e^{-6}$	186	3
Aggregated	I B	1	$2.18093e^{-7}$	$8.82690e^{-7}$	$1.22922e^{-6}$	$1.54e^{-7}$	$2.50e^{-5}$	$1e^{-10}$	117	3
		2	$2.18767e^{-7}$	$8.47592e^{-7}$	$1.59921e^{-6}$	$1.73e^{-7}$	$2.94e^{-6}$	$1e^{-10}$	184	2
		3	$2.79081e^{-7}$	$8.85570e^{-7}$	$2.58671e^{-6}$	$1.95e^{-7}$	$3.35e^{-5}$	$1e^{-10}$	220	3
	II B	1	$5.05758e^{-4}$	$3.33414e^{-3}$	$1.15199e^{-3}$	$4.43e^{-4}$	$7.33e^{-7}$	$1e^{-5}$	14	2
		2	$5.05423e^{-4}$	$3.53341e^{-3}$	$1.15171e^{-3}$	$4.55e^{-4}$	$7.90e^{-8}$	$1e^{-5}$	25	4
		3	$5.06846e^{-4}$	$3.69321e^{-3}$	$1.16161e^{-3}$	$4.68e^{-4}$	$7.94e^{-8}$	$1e^{-5}$	46	3

Results and discussion

This study develops a computational framework to simulate the flow of nanofluids on a wavy surface under Lorentz forces, considering diamond clusters. Figure 3 shows the flow chart of the numerical study with machine learning patterns of ANNs. Numerical results obtained via the Keller-Box method, integrated with a machine learning (ANN), demonstrate high predictive accuracy, as summarized in Tables 2 and 5. Aggregated cases (e.g., Scenario I B) achieved superior precision (MSE $\leq 10^{-7}$) and low validation-testing deviation but required more training time (117–220 epochs) and showed moderate overfitting behavior (MSE $\approx 10^{-5}$). The most inaccurate results were obtained in Scenario II B (MSE $\approx 10^{-4}$–10^{-3}), which was caused by an unduly small regularization parameter ($\mu \approx 10^{-10}$). Training ANN models took less than 3 s, and they provided predictions in less than 1 s. As Fig. 4 shows, surface waviness has a dual impact: aggregation improves thermal conductivity and the Nusselt number despite localized disturbances in the boundary layer; non-aggregated particles improve flow smoothness and pressure losses to the detriment of heat transfer with increasing sinusoidal condition (ε_T). In general, aggregation improves the thermal performance at the rise of pumping power, and dispersion increases the hydrodynamic efficiency, highlighting the need to trade off between surface geometry and the value of *M*. The significant engineering trade-off posed by nanoparticle aggregation is evident. In high heat flux applications (such as server chip cooling), a 30% increase in *Nu* is highly desirable, but the 25% increase associated with skin friction directly translates into higher pumping power. For the system designer, the decision should be based on the primary constraint, that is, if thermal efficiency is paramount and pumping power is readily available (e.g., in certain industrial exchangers), aggregated nanofluids are preferred. Conversely, in microfluidic or cooling systems of portable electronics, the lower drag of non-aggregated nanoparticles, despite a modestly lower *Nu*, may yield a better overall performance of the system coefficient. This difference is shown in the error histogram in Fig. 5, which identifies the predictive behavior between aggregated and non-aggregated nanoparticles. In the case of the Nusselt number, as shown in Fig. 5a, b, surface waviness (ε_T) increment together with a given particle type, surface waviness raises prediction errors in both cases; nevertheless, the aggregated particles have a stable, symmetric distribution, which denotes a balanced prediction and the presence of increased thermal pathways resistant to geometric disruptions. Non-aggregated cases exhibit skewed profiles, revealing systematic biases. Similarly, the gradient study Fig. 6a, b indicates that gradients remain constant during surface undulations in an aggregated setup, whereas in the non-aggregated setups, heat transfer is interrupted. This two-fold benefit of thermal homogeneity and magnetic stability makes aggregated nanoparticles better in systems that contain complicated

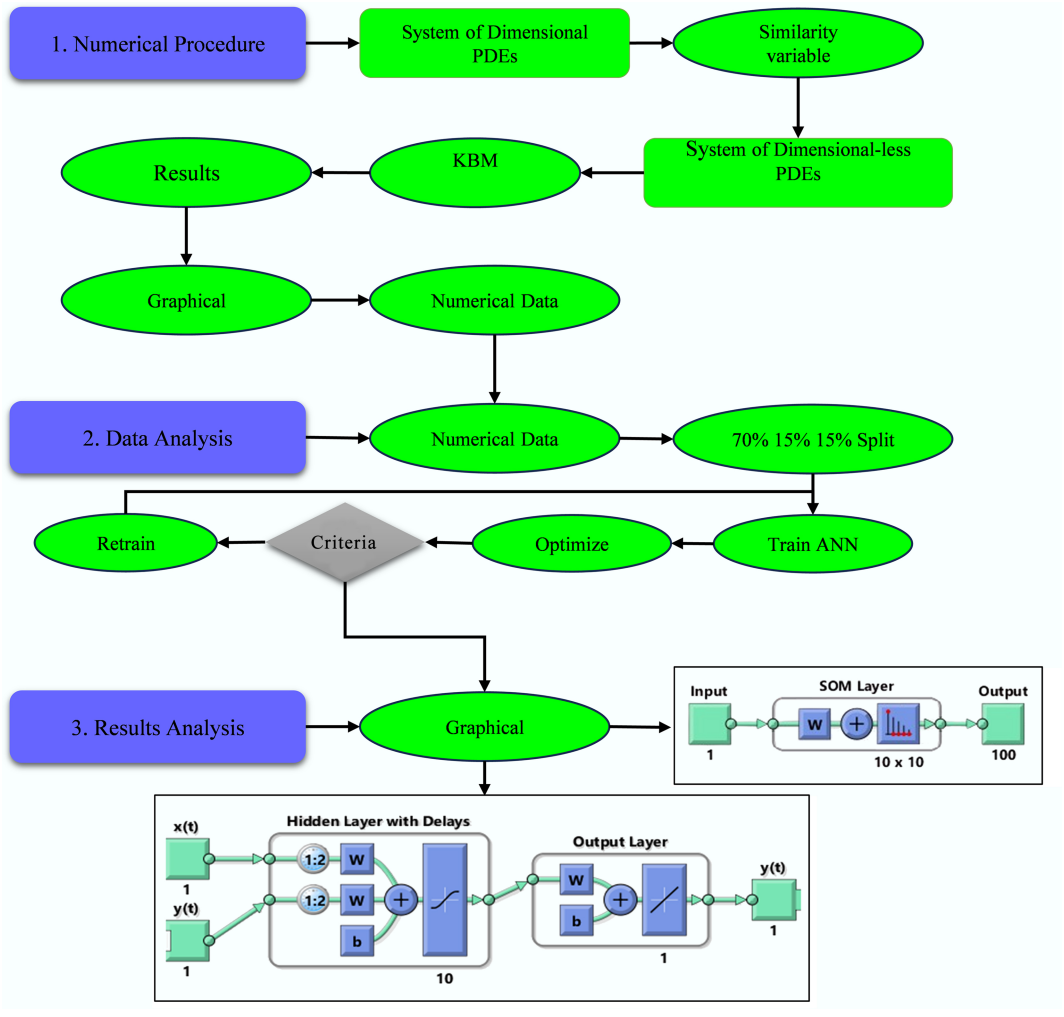

Fig. 3 Computational workflow for Integrated numerical modeling to validate predictions.

https://doi.org/10.48130/scm-0025-0013

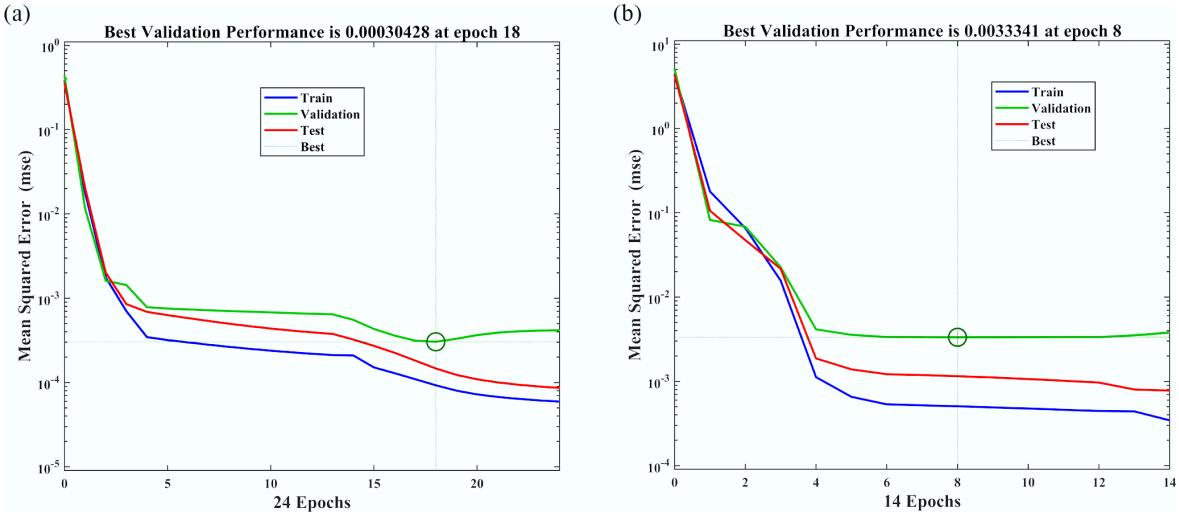

Fig. 4 Mean squared error (MSE) analysis for Nusselt number (*Nu*) vs sinusoidal parameter (ε_T) for comparing: (**a**) non-aggregated, and (**b**) aggregated nanoparticle configurations.

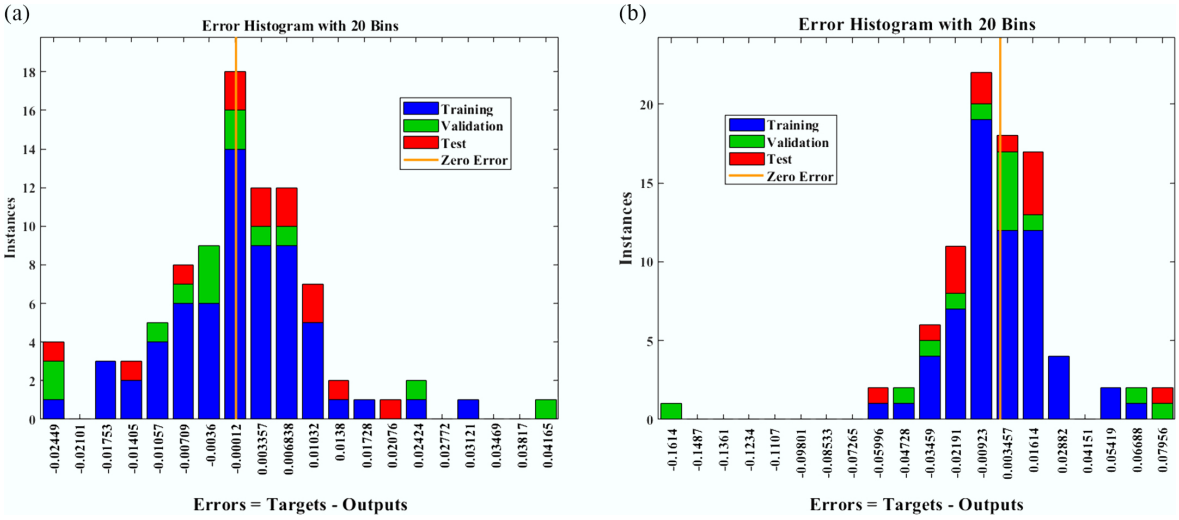

Fig. 5 Error histogram analysis for Nusselt number (*Nu*) vs sinusoidal parameter (ε_T) for comparing: (**a**) non-aggregated, and (**b**) aggregated nanoparticle configurations.

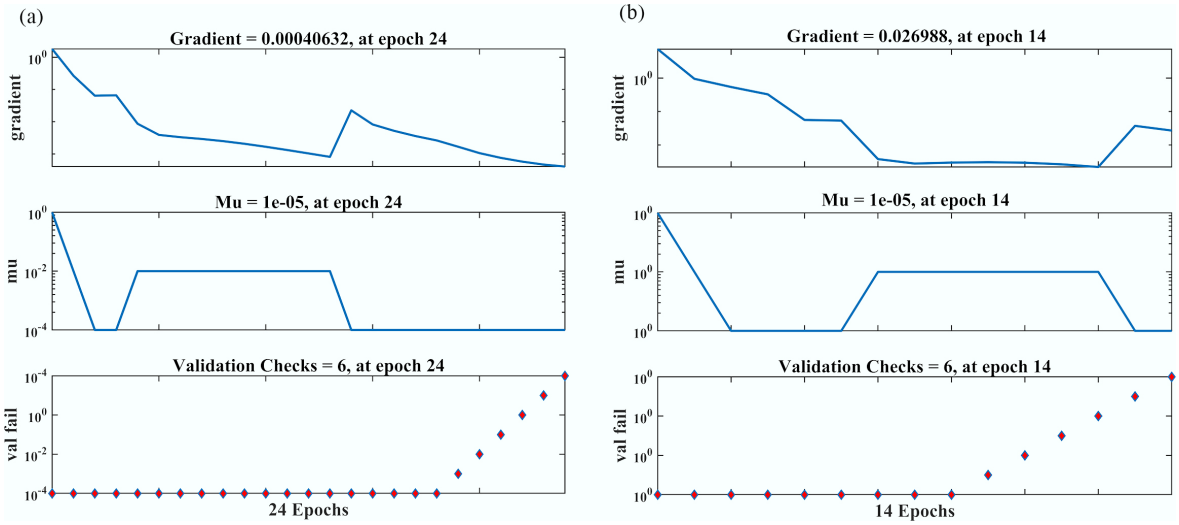

Fig. 6 Gradient validation analysis for Nusselt number (*Nu*) vs sinusoidal parameter (ε_T) for comparing: (**a**) non-aggregated, and (**b**) aggregated nanoparticle configurations.

geometries and magnetic interactions, although with a slight increase in viscosity.

Therefore, the idea of controlled aggregation can be proposed as a useful approach to increase the accuracy, stability, and reliability of the nanofluid under variable conditions. Correlation analysis indicates that different configurations of nanoparticles and various operating conditions interact differently. In the case of the Nusselt number, as shown in Fig. 7a, b, the effect of surface waviness on each configuration is smaller, but the correlations between the geometric variants are at a higher level because aggregated nanoparticles have networked structures that can absorb the disruptions of surfaces.

Consequently, aggregated nanoparticles offer an improved thermal uniformity for complex geometries, whereas non-aggregated ones perform better in strong magnetic fields, which yields a useful design framework for electronic cooling systems and solar collectors in which the geometric influence and magnetic influence need to be reconciled. The clustering analysis also shows that the arrangement of nanoparticles dominates the thermal performance in wavy surfaces. In the non-aggregated nanoparticles, as shown in Fig. 8a, c, both the self-organizing map (SOM) and Hits distributions are broadly distributed, which implies that there is no regular heat transfer at different values of ε_T. Aggregated nanoparticles in progression, as shown in Fig. 8b, d, on the other hand, present predictable and consistent heat transfer behavior with well-aligned SOM structures and compact Hits clusters. This is because of their interlinking channels, where the geometric anomalies are overcome through their inter-connectivity and hence transforming chaotic responses into uniform thermal responses, thus improving the performance in irregular flow wave surface and textured heat exchangers.

Figure 9a–d below shows how the strength of the magnetic field (M) influences the flow and thermal characteristics of non-aggregated or aggregated nanoparticle-containing nanofluids. Fig. 9a–d indicate that the skin friction coefficient (C_f) decreases significantly with increasing M and aggregated nanofluids always have higher C_f values in comparison with single phases because of increased viscosity and the higher viscosity against the Lorentz force. Aggregated nanoparticles have significantly larger (C_f) at M = 5.0 than non-aggregated nanoparticles by a factor of about 58%.

In contrast, Fig. 9c, d indicate that the Nusselt number, presented in all the cases, which is a measurement of the efficiency of heat transfer, rises and then subsequently falls, peaking in the range M = 2.0–3.0. Such a peak is more pronounced with non-aggregated nanofluids, as they have up to 22% increase in Nu because of the improved dispersion and lower isotropic viscosity. However, beyond M = 3.0, Nu in aggregated nanofluids decreases as the power of Lorentz forces overrides the convective motion. Additionally, the magnetic fields compress surface profiles, enhance Joule heating, and enhance chaining of particles, which are more pronounced in an aggregated system. Further, the initial rise in Nusselt number is due to Lorentz forces stabilizing the flow and suppressing instabilities, boosting convective heat transfer. Beyond an optimum point, the magnetic damping effect dominates, restricting fluid flow, and Joule heating becomes less effective, leading to a decline in surface heat transfer. Figure 10a–d illustrates the impact of the sinusoidal boundary parameter (ε_T) on skin friction C_f, and Nusselt number (Nu), of both types of nanoparticles. The growing surface undulation within the range of ε_T = 0.1–0.3, encourages flow separation and recirculation, which disrupts the thermal boundary layer and reduces its average thickness near the wall, leading to the observed decrease in Nu. Nonetheless, aggregated nanofluids have a consistent drag that is always approximately 25% higher, resulting in elevated viscosity. Equally, the reduction in Nu is between 15%–20%, but aggregate nanofluids retain up to 30% better heat transfer due to their higher thermal conductivity and efficient energy transfer. This represents a definite trade-off: non-aggregated nanofluids are suitable for low-drag systems, whereas aggregated ones are suitable for high-efficiency heat transfer. It is worth noting that diamond nanoparticles are costly but are not commonly utilized; however, their ultra-high thermal conductivity (1,000 W/m·K) and stability in MHD conditions make them highly suitable for novel thermal applications such as concentrated solar power and microelectronics. This 15%–30% performance disparity provides valuable

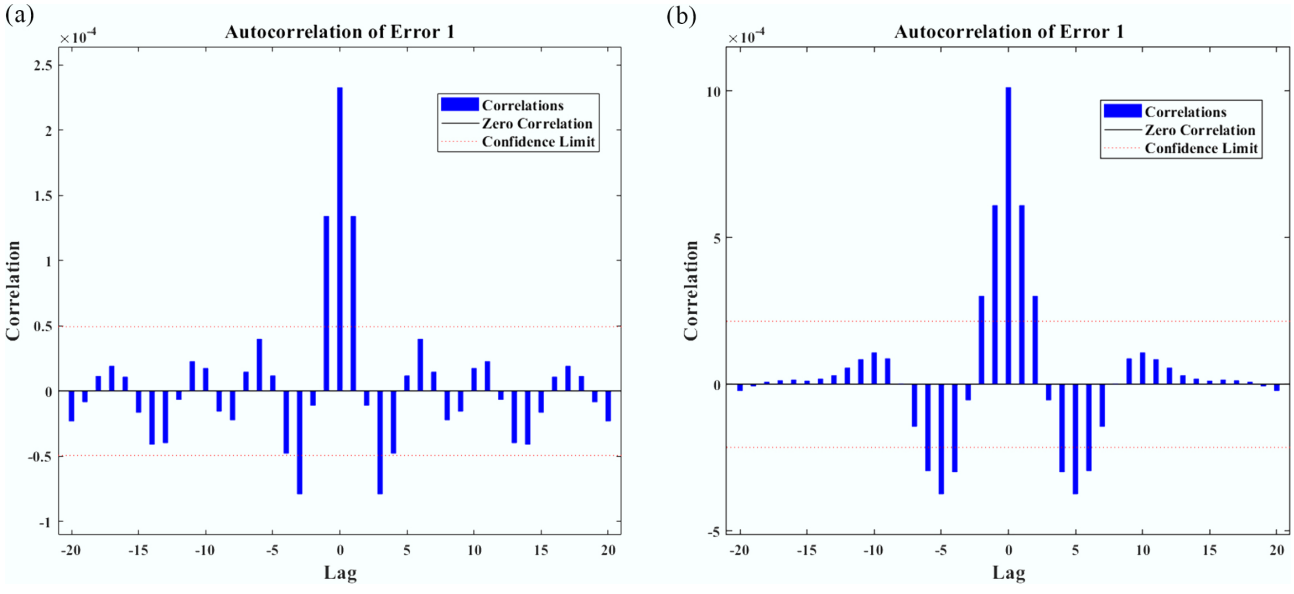

Fig. 7 Correlation patterns analysis for Nusselt number (Nu) vs sinusoidal parameter (ε_T) for comparing: (**a**) non-aggregated, and (**b**) aggregated nanoparticle configurations.

https://doi.org/10.48130/scm-0025-0013

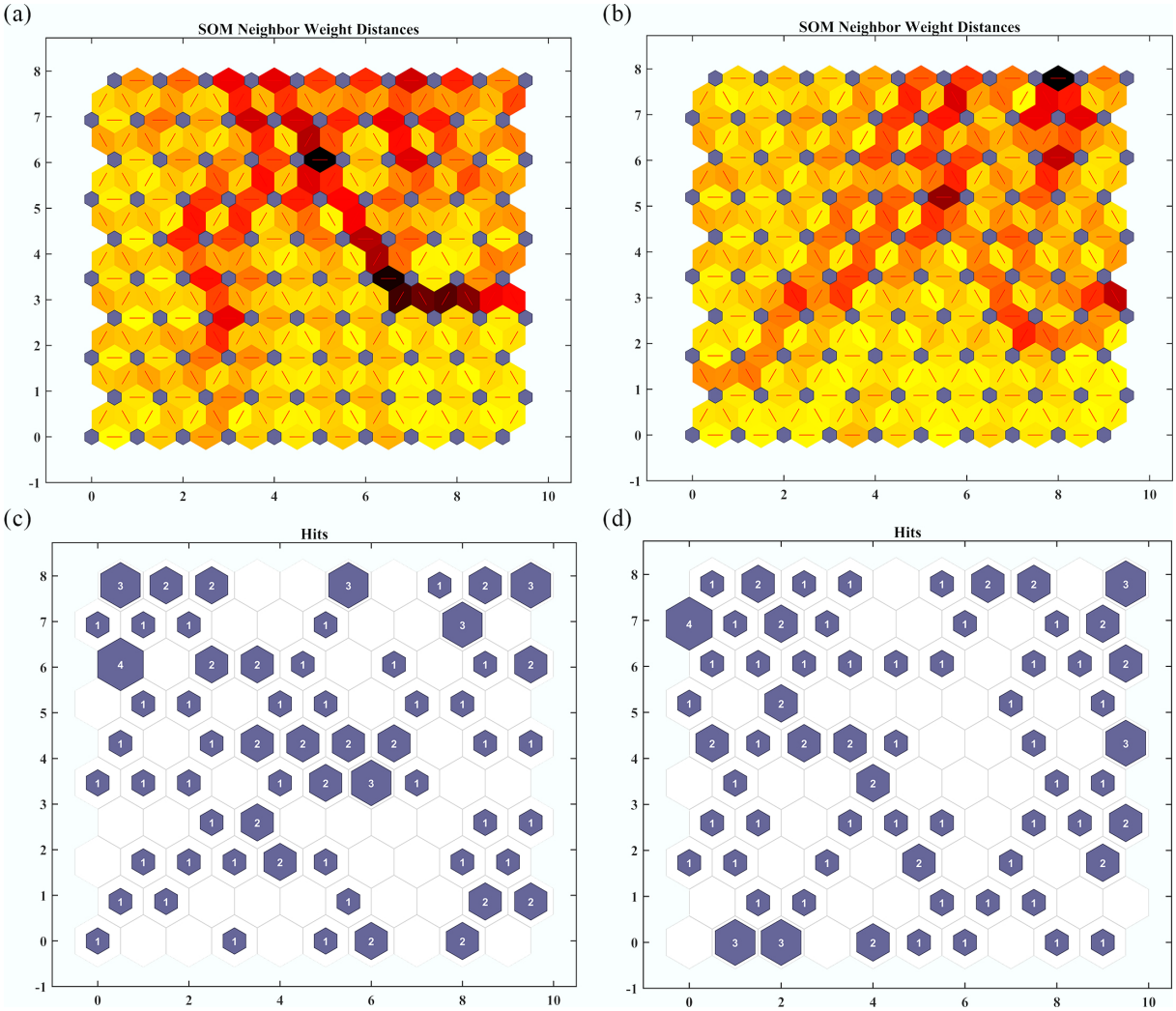

Fig. 8 Clustering analysis of the Nusselt number (*Nu*) as a function of the sinusoidal parameter (ε_T). **(a),** (**b**) SOM neighbor weight distance maps, and (**c),** (**d**) hit maps, comparing aggregated and non-aggregated nanoparticle configurations.

design insights and builds on previous findings by Shirvan et al.[15] and Sheremet et al.[16]. Although real-world complexities such as turbulence and dynamic particle dispersion may affect these results, the trends support the thermal advantages of aggregation in the high-performance nanofluid application.

Finally, Fig. 11a–d discusses the effect of the amplitude-to-wavelength ratio (α) on C_f and *Nu*. With the increase of α from 0.1 to 0.2, both quantities decrease by 6%–12% for C_f and 8%–15% for *Nu* due to surface waves, which disrupt the stability of the flow and weaken the thermal boundary layer.

Nevertheless, the effect of the aggregation eliminates these reductions: aggregated nanofluids have 15%–20% larger C_f because of higher viscosity and momentum diffusion, and 12%–18% larger *Nu* because of higher thermal conductivity and the development of conductive networks.

For example, the Nusselt number at *Nu* = 0.2 for the aggregated nanofluids reaches 0.75 compared to 0.6 for the unaggregated ones, representing a 17% improvement in performance, supporting the thermally favorable effect of nanoparticle aggregation. These observations indicate that non-aggregated nanofluids are better suited to systems that are drag-sensitive and need minimal surface perturbations, whereas aggregated nanofluids are beneficial in thermally sensitive systems, even when geometric constraints are present. The results are consistent with and build on prior studies conducted by Shirvan et al.[15], and by Sheremet et al.[16] by quantitatively demonstrating the trade-offs between hydrodynamic drag and heat transfer efficiency.

This research can be of great benefit to designing microfluidic cooling systems and compact heat exchangers, and in such cases, where it is necessary to optimize the balance between frictional loss and thermal performance. To alleviate the heat transfer reduction from surface waves, the set of Figs 10 and 11 suggest: (a) For systems using aggregated nanofluids, restrained waviness ($\varepsilon_T \approx 0.2$) can be tolerated as the conductive networks compensate. (b) For non-aggregated nanofluids, minimizing surface amplitude ($\alpha < 0.15$) is recommended unless the key objective is fluid mixing. (c) An optimum wavelength ratio (α) seems to be in the range of 0.1–0.15, corresponding to mixing enhancement with boundary layer distraction. Figure 12a–d shows the concentration of nanoparticles and aggregation vs the skin friction coefficient C_f and Nusselt number *Nu*, which brings into perspective significant trade-offs in nanofluid applications. As the value of ϕ increases from 0% to 4%, a greater increase in skin friction of about 40% and 25% is achieved with aggregated and non-aggregated nanoparticles, respectively.

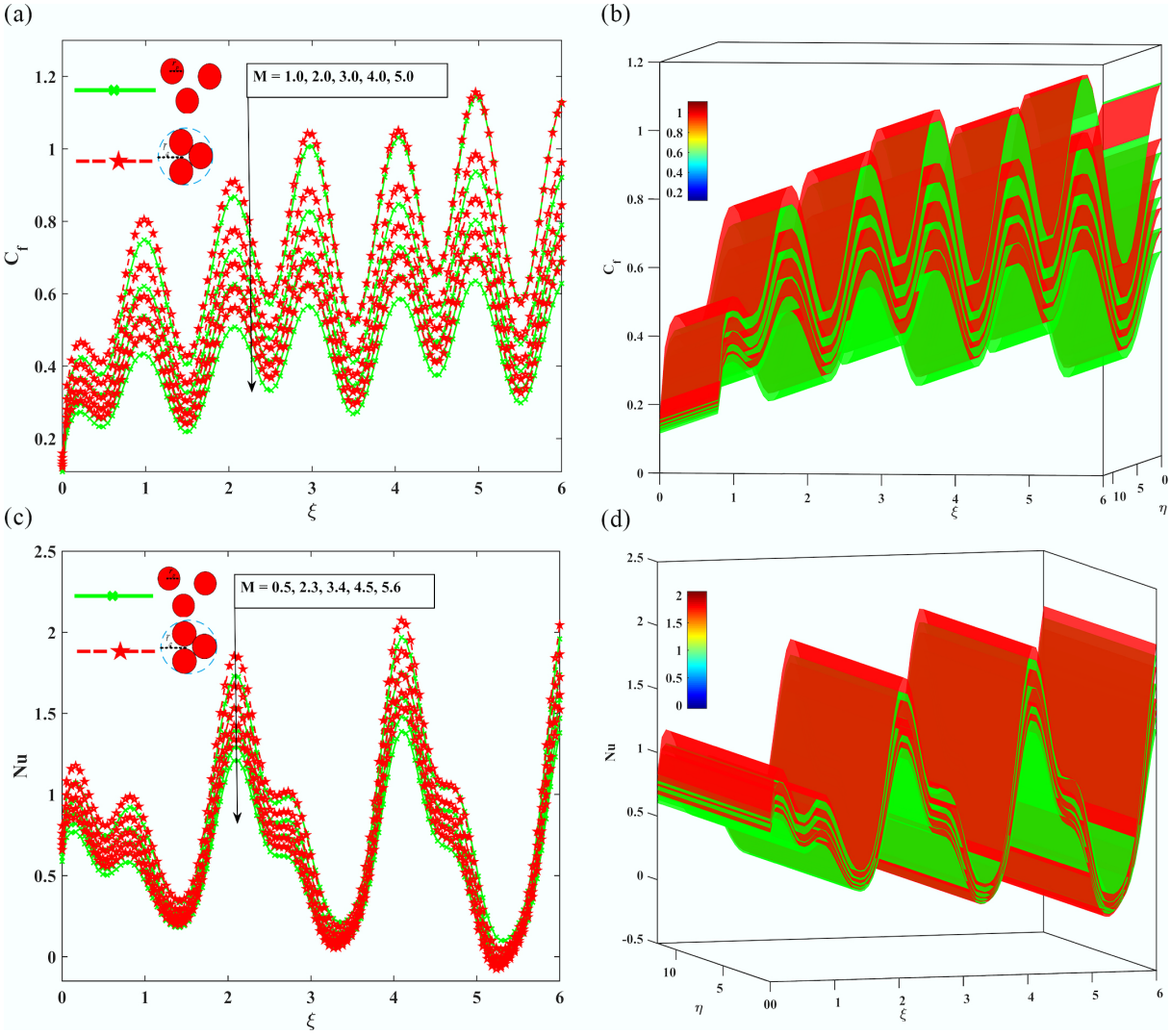

Fig. 9 The Impact of the magnetic parameter *M*, on (**a**), (**b**) skin friction coefficient C_f, and (**c**), (**d**) local Nusselt number *Nu*.

because the fluid viscosity and wall shear stress increase with ϕ, and the aggregate nanoparticles grow more rapidly because of their larger hydrodynamic size. A 4% overall concentration of ANPs allows for approximately 12% higher C_f, which is undesirable for drag-sensitive systems. Conversely, aggregated nanoparticles to a concentration of 50%, compared to non-aggregated ones to 30%, are much more effective in predicting the value of *Nu* since the process of particle clustering also facilitates thermal conductivity due to the formation of effective thermal conduction channels. Nevertheless, this enhancement levels off at elevated concentrations as a result of particle aggregation. Aggregated nanoparticles at 4% phi increased by about 15% in *Nu* compared to non-aggregated ones, hence at this ϕ, these nanoparticles are applicable in high heat flux applications like electronic cooling. The results are consistent with previous studies by Takabi et al.[14], and specifically measure the trade-off between flow resistance and thermal efficiency. Although an optimum ϕ of 2%–3% has been suggested to optimize the high yields of *Nu* with a manageable increment of C_f, in low-drag situations, non-aggregated nanoparticles are favored. Key assumptions include homogeneous particle distribution and homogeneous viscosity. Overall, the findings highlight the importance of balancing the aggregation state and the value of phi on the performance of the nanofluids to specific thermal hydraulic demands. It is significant to note that the present study is based on a numerical model. Although the simulations using the Keller-box method are well-established and the machine learning validation shows excellent consistency, experimental validation of the predicted trade-offs under combined MHD and wavy surface conditions would strengthen confidence in these guidelines for industrial application.

Conclusions

This study provides a numerical framework and design guidelines for optimizing thermal management systems using carbon-based diamond-water nanofluids on a wavy surface by integrating machine learning with the Keller-box method. The results indicate that carbon nano-materials clustering boosts thermal conductivity and leads to an up to 30% increase in Nusselt number, albeit a 25% increase in skin friction. Non-aggregated nanoparticles achieved a maximum improvement of 22% in heat transfer, accompanied by lower drag, at optimal magnetic field intensities (M = 2.3–3.4). The geometry of the surface had a substantial effect on the flow structure because too much waviness caused oscillatory flow, which reduced *Nu* by 15%–20%, and

https://doi.org/10.48130/scm-0025-0013

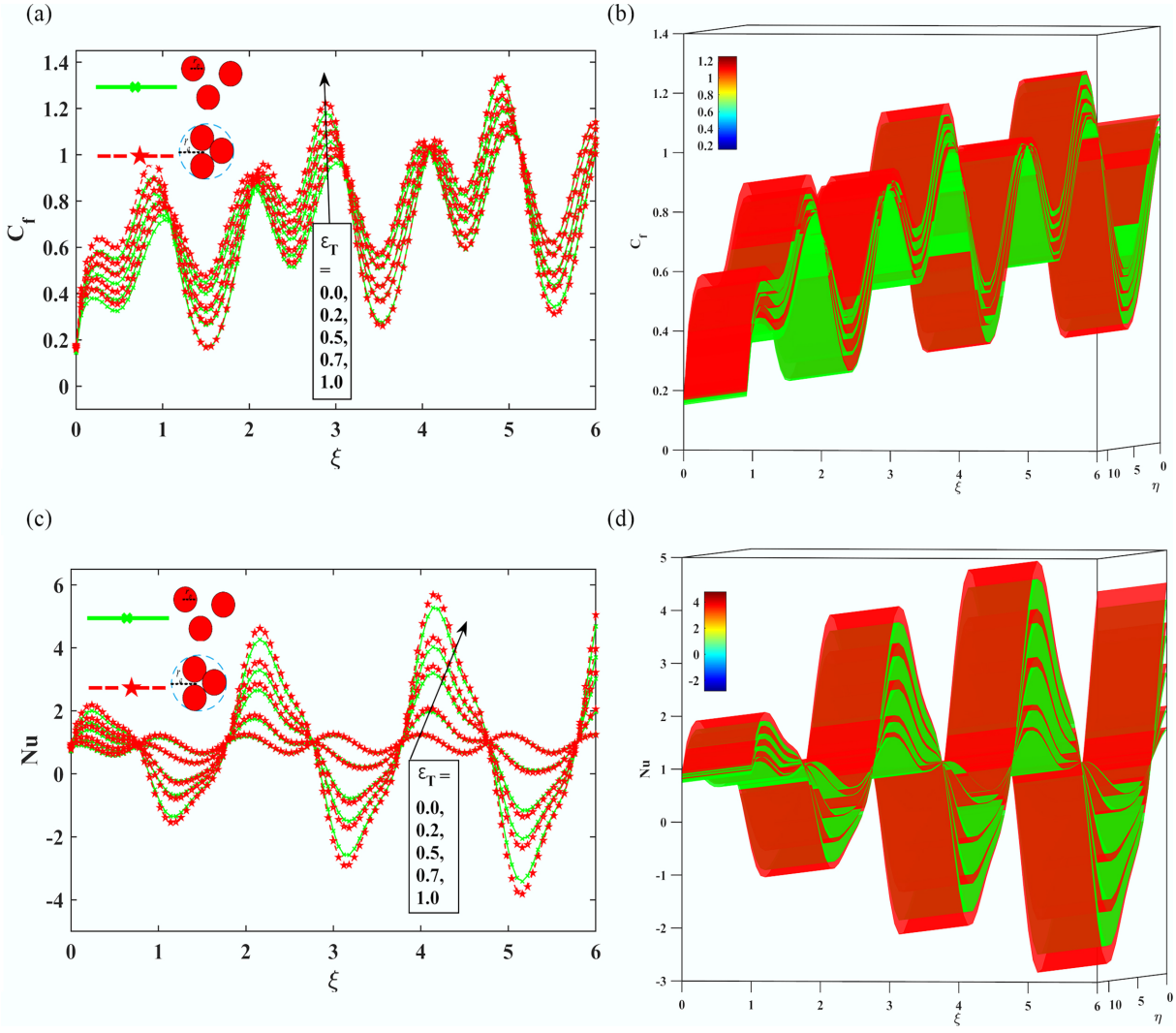

Fig. 10 The Impact of sinusoidal boundary parameter ε_T, on (**a**), (**b**) skin friction coefficient C_f, and (**c**), (**d**) local Nusselt number *Nu*.

aggregated nanoparticles alleviated this issue by keeping conductive paths open. Moderate magnetic fields ($M < 3.4$) were found to increase the movement, but stronger fields reduced the movement. Furthermore, the results show that aggregated nanofluids can accommodate a moderate sinusoidal boundary at ($\varepsilon_T \approx 0.2$) due to their enhanced conductive pathways, which counteract the reduction in heat transfer due to surface waves. Conversely, non-aggregated nanofluids advantageously maintain low surface amplitude ($\alpha < 0.15$) unless greater mixing is specifically required. Overall, aggregated carbon-based diamond nanofluids are best suited for high heat-flux applications, non-aggregated nanofluids for flow-sensitive systems, and magnetic field optimization between M = 2.0–3.0 provides the best trade-off. In addition, the most effective amplitude range is between 0.1 and 0.15, which offers a practical balance between improved mixing and limited boundary layers. The proposed KBM-ANN framework offers a reliable predictive tool for optimizing nanofluid-based thermal systems in complex geometries.

Future work and applications

Future studies will focus on experimental validation of the predicted thermo-hydraulic performance based on a prototype wavy surface under controlled Lorentz force conditions, ensuring consistency with the numerical results. Additionally, a compact multivariate optimization framework will be developed to balance *Nu*, C_f and pumping power for targeted applications such as wavy-channel heat sinks. Further interpretable machine-learning methods, such as symbolic regression, will be pursued to increase both predictive capability and physical insight. The extension of the study will also include hybrid diamond-metallic nanofluids and turbulent flow conditions. It is planned to extend the current research by developing a more detailed optimization approach with the ANN as a rapid surrogate within algorithms such as Genetic Algorithms to find Pareto-optimal combinations of the key parameters (M, ε_T, α in the aggregated state) to use in the practical engineering contexts.

Author contributions

The authors confirm their contributions to the paper as follows: all authors contributed to the conception and design of the study; material preparation, data collection, and analysis were performed by Danial Habib, Caiyan Qin, and Yue Yang; Danial Habib wrote the first draft of the manuscript, and all authors commented on previous versions of the manuscript. All authors reviewed the results and approved the final version of the manuscript.

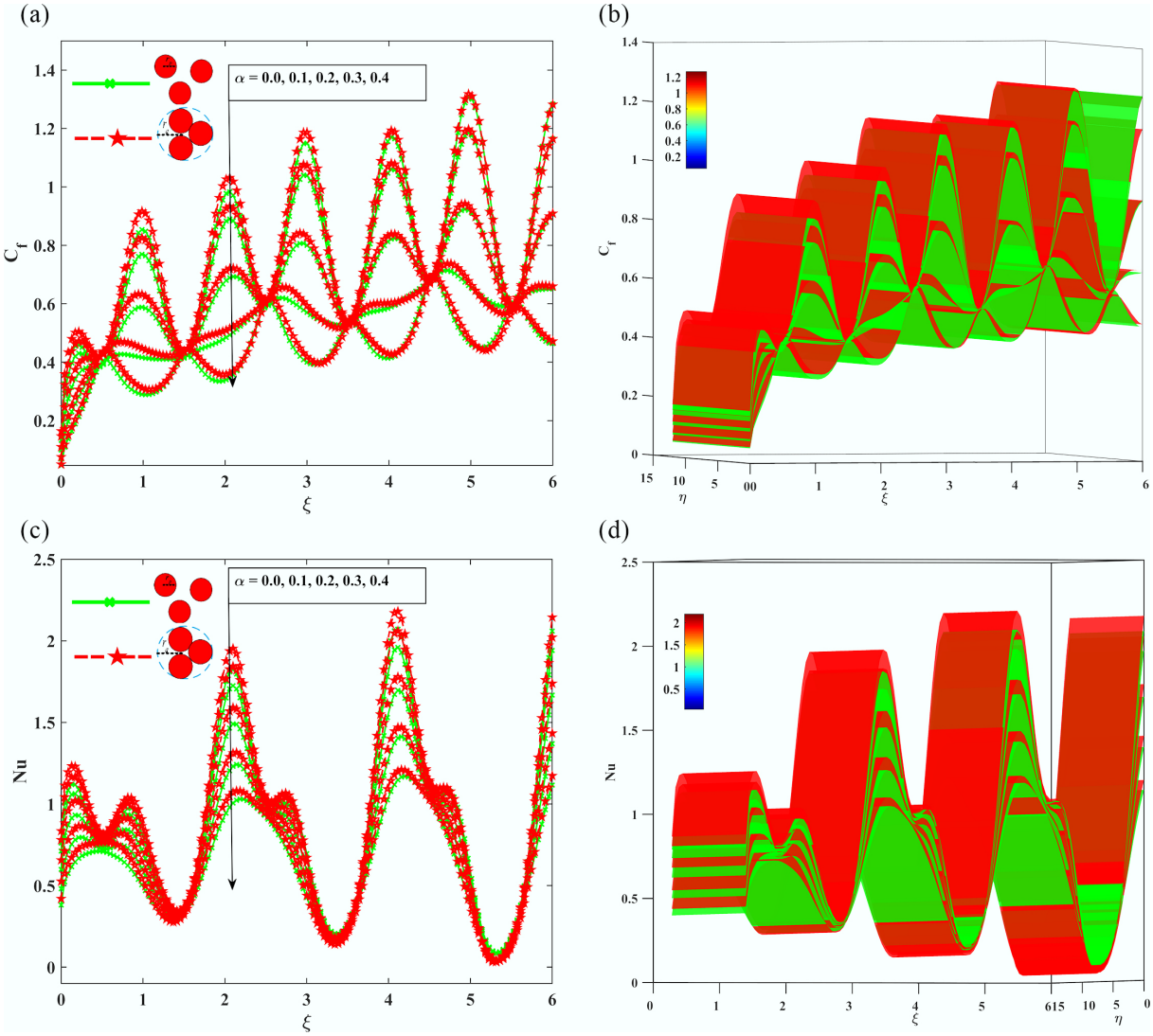

Fig. 11 The Impact of the wavelength ratio parameter α, on (**a**), (**b**) Skin friction coefficient C_f, (**c**), (**d**) local Nusselt number *Nu*.

Data availability

The datasets generated during and/or analyzed during the current study are available from the corresponding author on reasonable request.

Funding

This work was supported by the National Natural Science Foundation of China (Grant No. 52406079), General Program Funding (Grant No. JCYJ20250604145646062), and Stable Support Funding (Grant No. 20231130153633004) by the Shenzhen Municipal Science and Technology Innovation Bureau.

Declarations

Conflict of interest

The authors declare that there are no conflicts of interest related to this work.

Author details

[1]School of Robotics and Advanced Manufacturing, Harbin Institute of Technology, Shenzhen 518055, China; [2]Department of Mechanical Engineering and Science, Kyoto University, Kyoto, 615-8540, Japan

References

[1] Zhang Y, Xie Y, Zhao G, Liang Z, Shi J, et al. 2024. The important role of fluid mechanics in the engineering field. *Engineering Solutions to Mechanics, Marine Structures and Infrastructures* 1(2):421–445

[2] Doost SN, Zhong L, Su B, Morsi YS. 2016. The numerical analysis of non-Newtonian blood flow in human patient-specific left ventricle. *Computer Methods and Programs in Biomedicine* 127:232–247

[3] Shah J, Gupta SK, Sonvane Y, Davariya V. 2017. Review: Enhancing efficiency of solar thermal engineering systems by thermophysical properties of a promising nanofluids. *Renewable and Sustainable Energy Reviews* 77:1343–1348

[4] Timofeeva EV, Yu W, France DM, Singh D, Routbort JL. 2011. Nanofluids for heat transfer: an engineering approach. *Nanoscale Research Letters* 6(1):182

[5] Sohel MR, Saidur R, Khaleduzzaman SS, Ibrahim TA. 2015. Cooling performance investigation of electronics cooling system using

https://doi.org/10.48130/scm-0025-0013

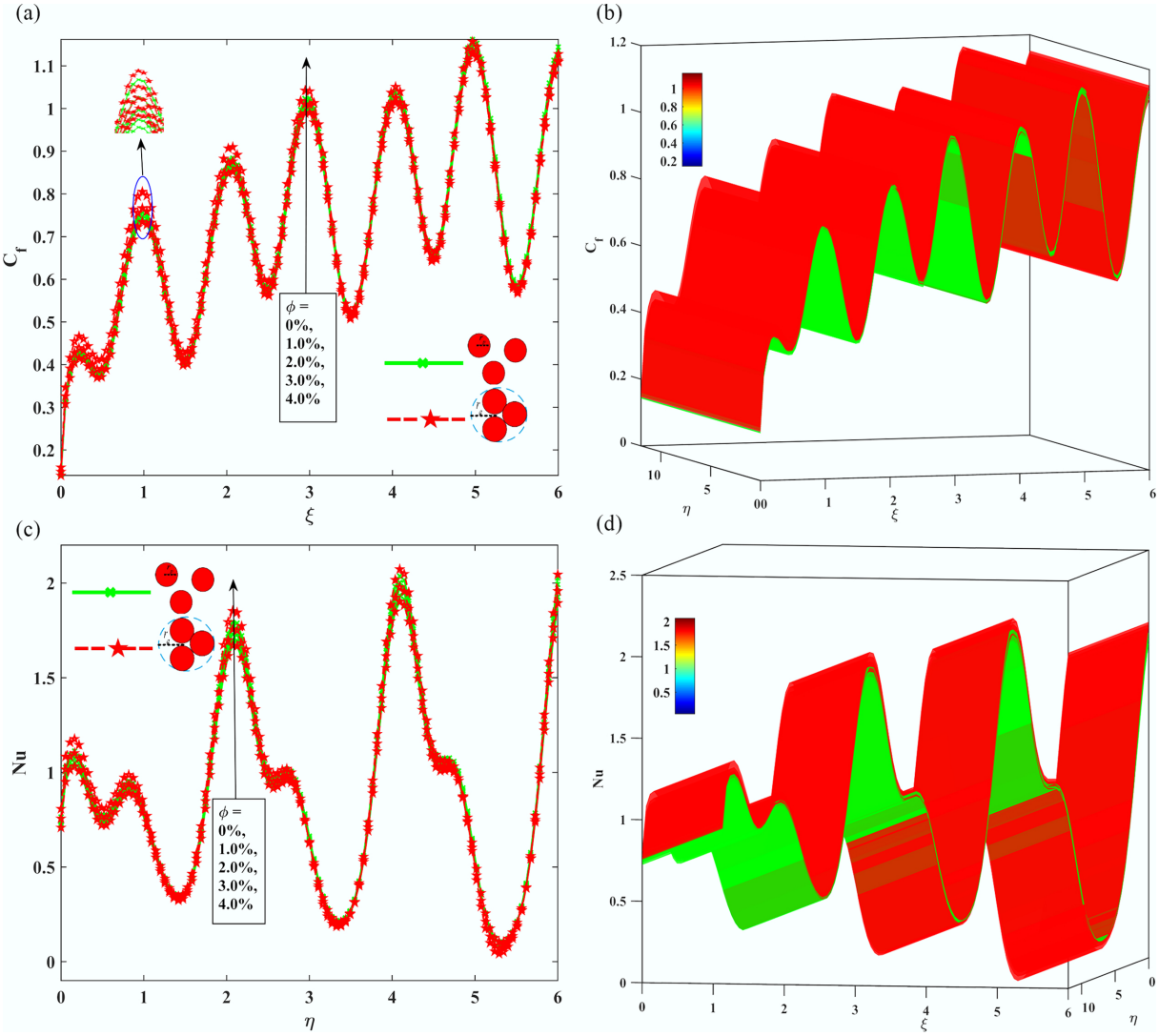

Fig. 12 The Impact of the concentration of NP ϕ, on (**a**, **b**) Skin friction coefficient C_f, (**c**, **d**) local Nusselt number *Nu*.

Al_2O_3–H_2O nanofluid. *International Communications in Heat and Mass Transfer* 65:89–93

[6] Santhosh N, Subramanyam Reddy A, Sivaraj R, Rushi Kumar B. 2025. Analyzing thermal performance of nanofluids in an inclined square enclosure with quadratic natural convection: applications in solar energy and electronic cooling. *Fluid Dynamics Research* 57(2):025506

[7] Choi SUS. 2025. Enhancing thermal conductivity of fluids with nanoparticles. *ASME 1995 International Mechanical Engineering Congress and Exposition, San Francisco, California, USA, 1995*. pp. 99–105 doi: 10.1115/IMECE1995-0926

[8] Yasmin H, Giwa SO, Noor S, Sharifpur M. 2023. Experimental exploration of hybrid nanofluids as energy-efficient fluids in solar and thermal energy storage applications. *Nanomaterials* 13(2):278

[9] Heidarshenas B, Yuan Y, El-Shafay AS. 2025. Advancements in 2D nanomaterial-enhanced nanofluids: stability, thermophysical properties, and industrial applications. *Powder Technology* 454:120687

[10] Ramzan M, Shaheen N, Saleel CA, Alazman I, Saeed AM, et al. 2025. A comparative analysis of nanoparticle aggregation and non-aggregation in a nanofluid flow over a cylinder influenced by prescribed surface temperature. *Multidiscipline Modeling in Materials and Structures* 21(4):830–849

[11] Wu SJ, Cai RR, Zhang LZ. 2025. Numerical simulation and modeling of nanoparticle aggregation effect on anisotropic effective thermal conductivity of nanofluids. *International Journal of Heat and Mass Transfer* 241:126681

[12] Madhukesh JK, Paramesh SO, Prasanna GD, Prasannakumara BC, Khan MI, et al. 2024. Impact of magnetized nanoparticle aggregation over a *Riga* plate with thermal radiation in water-Al_2O_3 based nanofluid flow. *ZAMM - Journal of Applied Mathematics and Mechanics* 00:e202300270

[13] Yang Z, Yu Q, Cui C, Xing H, Yin X, et al. 2025. Effect of aggregation on thermal conduction in ternary molten salt-based nanofluids: insights from a multiscale coupled MD–LBM method. *Energy Storage and Saving* 4(1):70–82

[14] Takabi B, Gheitaghy AM, Tazraei P. 2016. Hybrid water-based suspension of Al_2O_3 and Cu nanoparticles on laminar convection effectiveness. *Journal of Thermophysics and Heat Transfer* 30(3):523–532

[15] Milani Shirvan K, Ellahi R, Mamourian M, Moghiman M. 2017. Effects of wavy surface characteristics on natural convection heat transfer in a cosine corrugated square cavity filled with nanofluid. *International Journal of Heat and Mass Transfer* 107:1110–1118

[16] Sheremet MA, Cimpean DS, Pop I. 2017. Free convection in a partially heated wavy porous cavity filled with a nanofluid under the effects of Brownian diffusion and thermophoresis. *Applied Thermal Engineering* 113:413–418

[17] Iqbal MS, Mustafa I, Ghaffari A. 2019. Analysis of heat transfer enrichment in hydromagnetic flow of hybrid nanofluid along vertical wavy surface. *Journal of Magnetics* 24(2):271–280

[18] Iqbal MS, Mustafa I, Ghaffari A, Usman. 2021. A computational analysis of dissipation effects on the hydromagnetic convective flow of hybrid nanofluids along a vertical wavy surface. *Heat Transfer* 50(8):8035–8051

[19] Akter S, Hossain A, Islam MM, Molla MM. 2024. Finite difference simulation of natural convection of two-phase hybrid nanofluid along a vertical heated wavy surface. *Journal of Taibah University for Science* 18(1):2358548

[20] Munir S, Bin Turabi YUU. 2025. Impact of heated wavy wall and hybrid nanofluid on natural convection in a triangular enclosure with embedded cold cylinder under inclined magnetic field. *Arabian Journal for Science and Engineering* 50(6):4007–4020

[21] Alsabery AI, Chamkha AJ, Saleh H, Hashim I. 2017. Transient natural convective heat transfer in a trapezoidal cavity filled with non-Newtonian nanofluid with sinusoidal boundary conditions on both sidewalls. *Powder Technology* 308:214–234

[22] Karim A, Billah MM, Talukder Newton MT, Rahman MM. 2017. Influence of the periodicity of sinusoidal boundary condition on the unsteady mixed convection within a square enclosure using an Ag–water nanofluid. *Energies* 10(12):2167

[23] Mikhailenko SA, Sheremet MA, Pop I. 2019. Convective heat transfer in a rotating nanofluid cavity with sinusoidal temperature boundary condition. *Journal of Thermal Analysis and Calorimetry* 137(3):799–809

[24] Khosravi K, Eisapour AH, Rahbari A, Mahdi JM, Talebizadehsardari P, et al. 2023. Photovoltaic-thermal system combined with wavy tubes, twisted tape inserts and a novel coolant fluid: energy and exergy analysis. *Engineering Applications of Computational Fluid Mechanics* 17(1):2208196

[25] Foronda E, Ramírez-Gil FJ, Delgado-Mejía Á, Ballesteros LM, Rudas JS, et al. 2023. Thermal enhancement of heat sinks with bio-inspired textured surfaces. *Thermal Science and Engineering Progress* 46:102170

[26] Priyam A, Chand P. 2019. Experimental investigations on thermal performance of solar air heater with wavy fin absorbers. *Heat and Mass Transfer* 55(9):2651–2666

[27] Brodnianská Z, Kotšmíd S. 2023. Heat transfer enhancement in the novel wavy shaped heat exchanger channel with cylindrical *Vortex* generators. *Applied Thermal Engineering* 220:119720

[28] Hatami M, Jing D. 2017. Optimization of wavy direct absorber solar collector (WDASC) using Al_2O_3-water nanofluid and RSM analysis. *Applied Thermal Engineering* 121:1040–1050

[29] Ain QU, Ali Shah I, Alzahrani SM. 2024. Enhanced heat transfer in novel star-shaped enclosure with hybrid nanofluids: a neural network-assisted study. *Case Studies in Thermal Engineering* 61:105065

[30] Kamsuwan C, Wang X, Seng LP, Xian CK, Piemjaiswang R, et al. 2023. Enhancing performance of polymer-based microchannel heat exchanger with nanofluid: a computational fluid dynamics-artificial neural network approach. *South African Journal of Chemical Engineering* 46(1):361–375

[31] Zeeshan A, Khalid N, Ellahi R, Khan MI, Alamri SZ. 2024. Analysis of nonlinear complex heat transfer MHD flow of Jeffrey nanofluid over an exponentially stretching sheet *via* three phase artificial intelligence and Machine Learning techniques. *Chaos, Solitons & Fractals* 189:115600

[32] Islam T, Gama S, Afonso MM. 2024. Artificial neural network and response surface methodology-driven optimization of Cu–Al_2O_3/water hybrid nanofluid flow in a wavy enclosure with inclined periodic magnetohydrodynamic effects. *Mathematics* 13(1):1–45

[33] Bilal M, Maiz F, Farooq M, Ahmad H, Nasrat MK, et al. 2025. Novel numerical and artificial neural computing with experimental validation towards unsteady micropolar nanofluid flow across a Riga plate. *Scientific Reports* 15:759

[34] Ali B, Liu S, Liu HJ, Siddiqui MIH. 2025. Magnetohydrodynamics tangent hyperbolic nanofluid flow across a vertical stretching surface using Levengberg-Marquardt back propagation artificial neural networks. *Numerical Heat Transfer, Part A: Applications* 86(20):7116–7138

[35] Yahya Z, Mahmoud AM, Ali V, Khan O, Parvez M, et al. 2025. Material selection and optimization for hybrid Solar-Thermal plume Systems: a Machine learning approach to boost passive cooling and energy efficiency. *Thermal Science and Engineering Progress* 67:104097

[36] Mahanthesh B, Thriveni K. 2021. Nanoparticle aggregation effects on radiative heat transport of nanoliquid over a vertical cylinder with sensitivity analysis. *Applied Mathematics and Mechanics (English Edition)* 42(3):331–346

[37] Loksupapaiboon K, Kamma P, Phromjan J, Phakdee S, Promtong M, et al. 2025. Simulation-driven optimization of direct solar dryers for household use: a combined CFD and ANN-GA approach. *Thermal Science and Engineering Progress* 67:104112

[38] Sheremet MA, Pop I. 2015. Natural convection in a wavy porous cavity with sinusoidal temperature distributions on both side walls filled with a nanofluid: buongiorno's mathematical model. *Journal of Heat Transfer* 137(7):072601

[39] Sundar LS, Singh MK, Sousa ACM. 2016. Enhanced thermal properties of nanodiamond nanofluids. *Chemical Physics Letters* 644:99–110

[40] Mackolil J, Mahanthesh B. 2021. Inclined magnetic field and nanoparticle aggregation effects on thermal Marangoni convection in nanoliquid: a sensitivity analysis. *Chinese Journal of Physics* 69:24–37

[41] Prasher R, Phelan PE, Bhattacharya P. 2006. Effect of aggregation kinetics on the thermal conductivity of nanoscale colloidal solutions (nanofluid). *Nano Letters* 6(7):1529–1534

[42] Evans W, Prasher R, Fish J, Meakin P, Phelan P, et al. 2008. Effect of aggregation and interfacial thermal resistance on thermal conductivity of nanocomposites and colloidal nanofluids. *International Journal of Heat and Mass Transfer* 51(5–6):1431–1438

[43] Salahuddin T, Khan M, Mahmood Z, Awais M, Al Alwan B, et al. 2025. Effect of varying the temperature dependent viscosity of Maxwell nanofluid flow near a sensor surface with activation enthalpy. *Chaos, Solitons & Fractals* 194:116247

[44] Keller HB. 1971. A new difference scheme for parabolic problems. In *Numerical Solution of Partial Differential Equations–II*. US: Academic Press. pp. 327–350 doi: 10.1016/B978-0-12-358502-8.50014-1

[45] Cebeci T, Bradshaw P. 1988. *Physical and Computational Aspects of Convective Heat Transfer*. New York, NY: Springer doi: 10.1007/978-1-4612-3918-5